JOURNAL OF MATERIALS SCIENCE **34** (1999) 65–69

Coarsening of needle-shaped apatite crystals in $SiO_2 \bullet Al_2O_3 \bullet Na_2O \bullet K_2O \bullet CaO \bullet P_2O_5 \bullet F$ glass

R. MÜLLER, L. A. ABU-HILAL*, S. REINSCH
Bundesanstalt für Materialforschung und -prüfung BAM, Berlin, Germany

W. HÖLAND
IVOCLAR AG, Liechtenstein
E-mail: ralf.mueller@bam.de

Coarsening of needle-shaped apatite crystals was studied in a $SiO_2 \bullet Al_2O_3 \bullet Na_2O \bullet K_2O \bullet CaO \bullet P_2O_5 \bullet F$ glass. Crystal numbers and size distributions were measured by image analysis of electron micrographs obtained from slightly etched fractures of powder compacts sintered from differently annealed glass powders. Results indicate that the growth of apatite needles is controlled by diffusion-limited Ostwald ripening. Thus, the mean needle diameter and length increase with $t^{1/3}$ while the crystal number decreases with t^{-1} due to a constant volume fraction of apatite. An invariant reduced size distribution could be found for the diameters. The measurement of needle lengths is affected by several difficulties (e.g. random needle orientation).

1. Introduction

Special glass-ceramics are widely used in the field of restorative dentistry due to their well tailorable properties (e.g. mechanical strength, chemical resistance, material wear, color, translucency) which can be tuned close to the properties of natural tooth. Precursor materials, which are used by dental technicians to fabricate glass-ceramic dental restorations by casting, pressing and sintering of glass powders, require a special combination of properties and a particular viscosity.

Against this background, the complex crystallization kinetics of multicomponent silicate glasses is a matter of current interest. Liquid phase separation phenomena, the competitive growth and dissolution of various crystal phases, often controlled by diffusion-flow, small crystal sizes and small maximum volume fractions are frequently observed for these cases. During the asymptotic stage of overall crystallization, larger crystals can grow at the expense of smaller ones while the crystal volume fraction remains constant. As a result of this coarsening phenomenon, known as Ostwald ripening, the interfacial energy of the system is reduced [1–3].

In the present paper, the coarsening of needle-shaped apatite, in $SiO_2 \bullet Al_2O_3 \bullet Na_2O \bullet K_2O \bullet CaO \bullet P_2O_5 \bullet F$ glass containing additions of CeO_2, Li_2O, ZrO_2, B_2O_3 and TiO_2 is studied as an example.

2. Experimental

2.1. Samples

Parent glasses were conventionally melted, fritted, milled, and sieved to $<90\ \mu$m. Two glasses of similar composition were used (Table I). Glass powders were variously annealed in order to obtain needle-shaped apatite crystals of various numbers and sizes. Samples were isothermally treated at 1050 °C for 10 min, 20 min, 30 min, 1 h, 2 h, and 3 h. The resulting partially crystallized powder compacts were crushed and milled, formed into plates and exposed to a further sintering treatment. This step simulates the sintering of the partially crystallized glass powder to dense glass-ceramic compacts of complex shape for restorative dentistry. The sintering step includes heating at 60 K min^{-1} to 1000 °C, holding 1 min, and quenching in air. Due to the short sintering time, this step has a minor influence on crystal number and size. Finally, the sintered compacts were embedded in synthetic resin, cut and polished perpendicular to their former bottom plane, and etched for 10 s in 2.5% HF.

2.2. Measurement

All samples were studied by scanning electron microscopy ("DSM 962", Zeiss, Germany). Representative electron micrographs were scanned for kinetic studies by image analyzing ("IMAGE C", Imtronic, Germany). Each crystal was individually selected and measured to avoid misinterpretations. Crystals clipped by the margin of the micrographs were solely used for counting crystal number and diameter. Sample preparation and measurement have been performed independently for both glasses to realize experimental errors.

3. Results

Two main crystal phases occur in the present case. First, numerous small needle-shaped apatite crystals showing

* On a trainee leave from the University of Jordan.

TABLE I Batch composition of the used glasses in mol %

	SiO_2	Al_2O_3	Na_2O	K_2O	CaO	ZrO_2	P_2O_5	F	CeO_2	Li_2O	B_2O_3	TiO_2
Glass 1	61.8	12	10.4	7.5	3.2	1	0.6	2.2	0.2	1	0.3	-
Glass 2	61.5	9.4	9.2	7.7	6.0	0.5	1.9	2.5	0.3	0.5	0.3	0.2

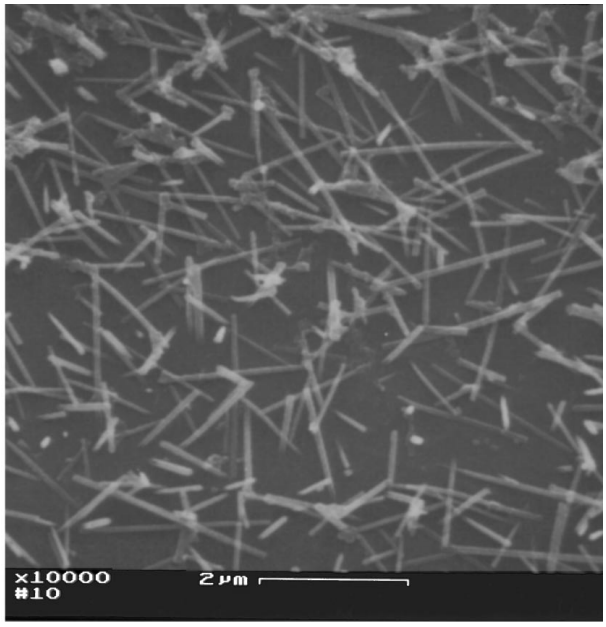

Figure 1 Scanning electron micrograph of a thermally treated glass powder.

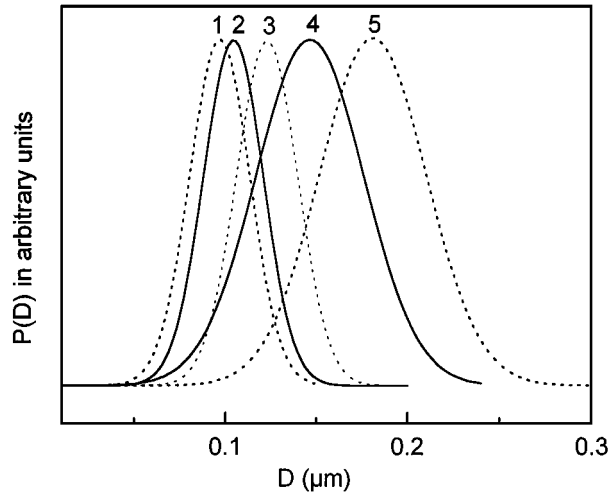

Figure 2 Distribution of diameters, $P(D)$, of apatite crystals isothermally treated at 1050 °C for 20 min (curve 1), 30 min (2), 1 h (3), 2 h (4) and 3 h (5).

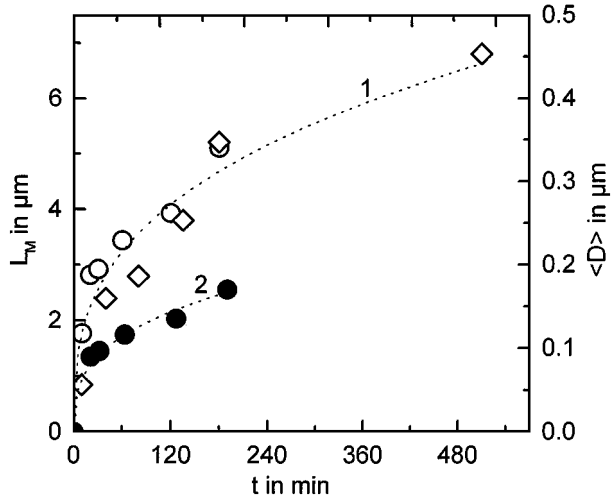

Figure 3 Maximum length, L_M (○: glass 1, ◇: glass 2, curve **1**: $L_M = 0.83t^{1/3}$) and mean diameter, $\langle D \rangle$, of apatite needles (●: glass 1, curve **2**: $\langle D \rangle = 0.03t^{1/3}$) as a function of time, t, for isothermal annealing at 1050 °C.

hexagonal cross-section are evident. Previous work indicates a volume-induced nucleation of these needles, probably related to liquid phase separation phenomena [4]. Secondly, a few, but larger, leucite crystals have grown from the former glass particle surface. Further, a few unidentified crystals were found in some cases [8].

In the present paper, however, attention is focused on the apatite needles only. More detailed crystallization studies are described elsewhere [4–6]. SEM micrographs showing only apatite needles were used for kinetic studies. One example is given in Fig. 1. One should note that visible apatite needles stand out of the bulk material as a result of etching. The material contrast of needles often fades out along one needle direction. This effect is caused for needles that reach down into the ground due to the limited penetration depth of the electron beam. For the sake of simplification, the needle size is characterized by its length, L, and its diameter, D, in the following sections.

The diameter of apatite needles, D, could be directly measured from the micrographs. D was taken from the more pronounced part of the needles to avoid errors related to electron charge or fading-out effects. Fig. 2 shows the size distribution, $P(D)$, for various thermally treated samples. For each sample, the absolute number of crystals belonging to 10 different classes of size was counted. The class width, ΔD, was taken as a tenth of the maximum diameter. In order to compare $P(D)$ for differently annealed samples of different ΔD, the crystal numbers are normalized. The mean diameter, $\langle D \rangle$, is shown in Fig. 3 (full points, curve 2).

The length of apatite needles, L, can not be directly measured due to needle orientation. Instead, the frequency distribution of the apparent needle length, $P(L_a)$, is shown in Fig. 4 for various isothermally treated samples. $P(L_a)$ shows a sigmoidal shape asymmetrically increased at the lower side. The higher side of $P(L_a)$, represents more needles oriented close to the observation plane were $L \approx L_a$ is valid.

Hence the maximum values of L_a and L coincide. This maximum value, L_M, is shown in Fig. 3. The data scatter, caused by the statistical nature of selecting the largest needle is indicated by a comparison of data for glass 1 (○) and glass 2 (◇).

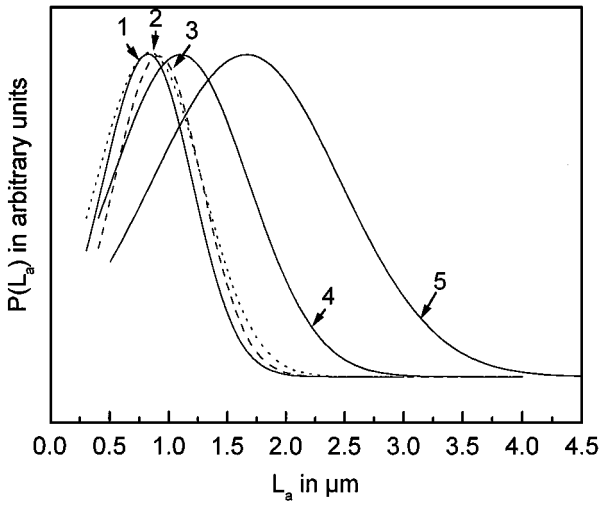

Figure 4 Distribution of apparent needle lengths, $P(L_a)$, for isothermal treatment. See Fig. 2 for curve number.

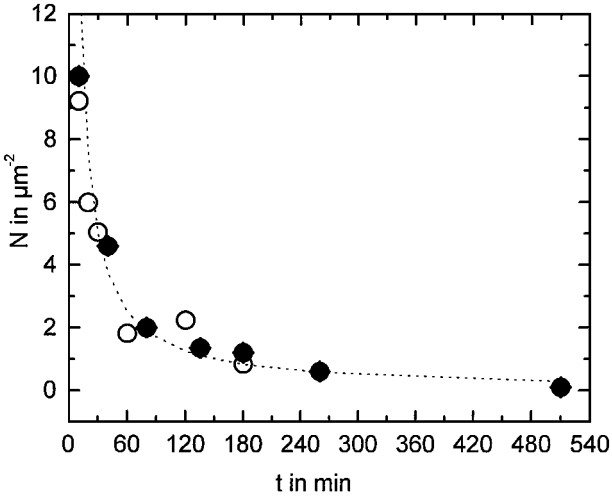

Figure 5 Number of crystals per unit square as a function of time for isothermal treatment at 1050 °C. ○: glass 1, ●: glass 2.

The number of crystals per unit square, N, counted from the electron micrographs for each sample is shown in Fig. 5. Data points represent an area of 88 μm^2. The data scatter between glasses 1 and 2 illustrates related experimental errors.

4. Discussion

If precipitated particles are small and interact by diffusional flow, their size distribution is affected by Ostwald ripening causing large particles to grow at the expense of small ones, usually in the asymptotic stage of precipitation [e.g. 1–3]. The related driving force is the energy yield due to the reduction of the total interface area. In the classical theory of Ostwald ripening, this driving force is implemented by the Gibbs–Thomson or Thomson–Freundlich solubility relationship [2]:

$$C_{\alpha\beta}(r) = C_{\alpha\beta}(r = \infty) \cdot \exp\left\{\frac{2V_m\sigma}{RT \cdot r}\right\} \qquad (1)$$

(V_m: molar volume of the precipitate, r: its radius, σ: surface tension, T: absolute temperature, R: gas constant, $C_{\alpha\beta}(r)$: composition of the α matrix in equilibrium with a spherical particle of β). For diffusion-limited growth, typical kinetic phenomena can be expected in the asymptotic stage: (i) a growth of the mean particle size according to $\langle R\rangle \sim t^{1/3}$, (ii) a constant volume fraction of the precipitate resulting in a decrease of particle number with $N \sim t^{-1}$, and (iii) a time-invariant distribution of the reduced particle size, $P(R/\langle R\rangle)$ [e.g. 3].

Although the classical theory is based on small spherical particles (Equation 1), coarsening is known for non-spherical crystal grains in the micrometer range as well. As an example, the coarsening kinetics for a two-phase alumina–zirconia composite could be well fitted in terms of diffuse-interface-field computer simulations without assuming spherical particles. Even in this case, all kinetic features for diffusion-limited growth, mentioned above, were found [7]. Thus, it should not lead to confusion that apatite needles, under consideration here, are far from spherical shape showing hexagonal cross-sections and are thus bound by plane surfaces.

4.1. Diameter, *D*

It can be discussed most easily in the case of diameters whether the observed growth kinetics of apatite needles is controlled by Ostwald ripening. In Fig. 3 the mean diameter, $\langle D\rangle$, is shown as a function of time, t, for isothermal annealing at 1050 °C. $\langle D\rangle$ follows a $t^{1/3}$ growth law. A similar behavior was previously found for glass 2 in the case of thermal treatments at 1000 °C [6]. The distribution of the reduced diameter, $P(D/\langle D\rangle)$, is shown in Fig. 6. The shape of this distribution is not essentially influenced by the applied isothermal treatments. Thus, both the growth of the mean diameter and the change of its reduced size distribution indicate diffusion-limited Ostwald ripening.

4.2. Length, *L*

For the needle length, L, the situation is more complex because L can not be directly measured. This is caused by two difficulties. First, due to the random orientation of the needles, only an apparent length, L_a, can be

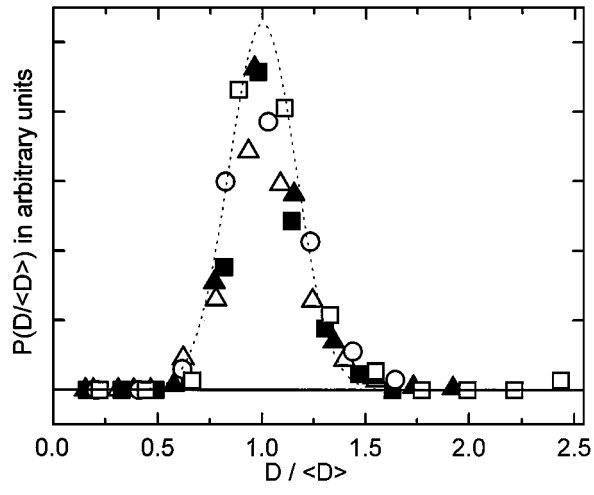

Figure 6 Frequency distribution of the reduced diameter $P(D/\langle D\rangle)$. Points: △: 20 min, ▲: 30 min, ■: 1 h, ○: 2 h, ❑: 3 h.

measured directly. L_a depends on the angle between the needle's axis and the observation plane, φ. Secondly, electron micrographs, used in this study, represent information from a thin sample layer. Its thickness, h, mainly results from sample etching and is slightly enhanced by the permeability of the electron beam into the glassy matrix. In the present case, $h \approx 2 \ldots 5\,\mu$m might be expected [8]. Concerning the mean value of the true needle length, $\langle L \rangle$, two limiting cases are given:

$\langle L \rangle \gg h$ In this case, only a small part of each needle was made visible by etching, except needles oriented almost parallel to the observation plane ($\varphi \approx 0$). For $\varphi \neq 0$, L_a does not depend on L but on h according to $L_a = h \cdot \cot \varphi$. Thus, the growth of needles can not influence the size distribution of the apparent length, $P(L_a)$. Only almost parallel oriented crystals ($\varphi \approx 0$) will increase $P(L_a)$ at its large side if the mean needle length is increased due to prolonged thermal treatment.

$\langle L \rangle \ll h$ In this case, most of crystals are completely visible and $L_a = L \cos \varphi$ is valid. Only a small part of crystals reach down into the ground beyond the penetration depth of the electron beam. The number of crystals oriented rather parallel to the observation plane ($\varphi \approx 0$), however, can be falsified by washing-out of crystals during etching or increased by sticking previously removed needles to the sample surface.

Hence, the observed distribution of apparent lengths, $P(L_a)$, can be utilized to calculate that of true lengths, $P(L)$, only if $\langle L \rangle \ll h$ is valid, φ is uniformly distributed, and washing-out phenomena can be neglected. In such a case, the total number of needles, N, can be subdivided into $z = \pi/2\Delta\varphi$ classes of differently oriented needles, defined by φ and $\Delta\varphi$. The same distribution of true length, $P(L)$, is given for all classes. However, each class causes different apparent length distribution, $P(\varphi, L_a)$ due to different needle orientation. For $\Delta\varphi \to 0$ it is:

$$P(L_a) = \frac{2}{\pi} \int_0^{\pi/2} P(\varphi, L_a)\, d\varphi \qquad (2)$$

If $P(L)$ is assumed to be of the Gaussian type, where $\langle L \rangle$ is the mean value of the true length and σ is its standard deviation, $P(\varphi, L_a)$ is:

$$P(\varphi, L_a) = \frac{1}{\sigma\sqrt{2\pi}} \exp\left\{ -\frac{(L - \langle L \rangle \cdot \cos\varphi)^2}{2\sigma^2 \cos^2 \varphi} \right\} \qquad (3)$$

Based on Equations 2 and 3, $P(L_a)$ can be calculated by numerical integration. Fig. 7 illustrates this procedure for $z = 10$ (see dashed and solid curves). Experimental $P(L_a)$ data points could be well fitted for the sample annealed 20 min at 1050 °C because $\langle L \rangle \ll h$ is valid most easily for this case. The slight asymmetric increase of $P(L_a)$ for small L_a can thus be attributed to needle orientation phenomena. For longer annealing time,

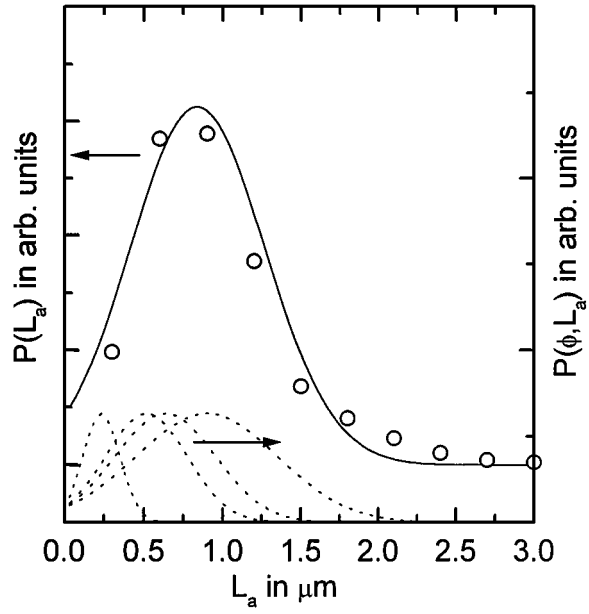

Figure 7 Solid curve: Distribution of apparent length, $P(L_a)$, calculated from Equations 2 and 3 for $\langle L \rangle = 0.8\,\mu$m and $\sigma = 0.45\,\mu$m; Dashed curves: $P(\varphi, L_a)$ calculated from Equation 3 for $\varphi = 0$, 45, 65 and 85° (shown for the sake of illustration); ❍: experimental $P(L_a)$ data for the sample annealed at 1050 °C for 20 min.

where $\langle L \rangle \ll h$ is more questionable, the fit of $P(L_a)$ was more difficult, particularly for the larger side of $P(L_a)$.

Despite this problem, the fitted mean values of $\langle L \rangle$ were always close to the most frequent apparent length. Therefore, the described fitting was utilized to estimate $\langle L \rangle$ for all thermal treatments, while no further use of fitted parameters was made. Results obtained in this way are shown in Fig. 8. A fit of $\langle L \rangle$ to a $t^{1/3}$ -growth law seems possible, but much less confidently than that in Fig. 3 for $\langle D \rangle$. The same growth law for $\langle D \rangle$ and $\langle L \rangle$ indicates that the equilibrium crystal shape, given by the Gibbs–Wulff-construction, remains unchanged during coarsening.

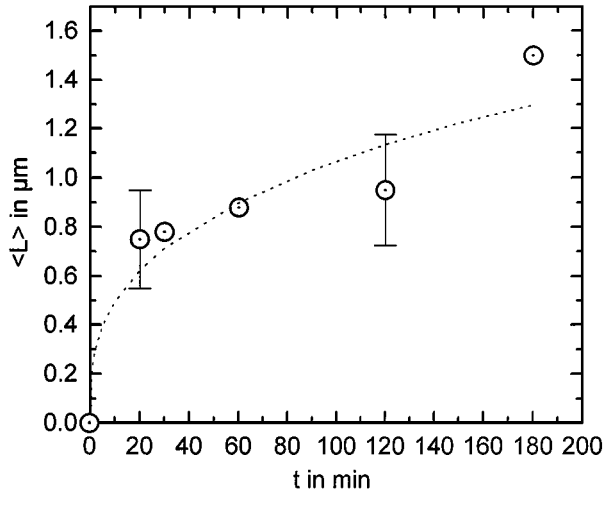

Figure 8 Mean crystal length, $\langle L \rangle$ as a function of time, t, for annealing at 1050 °C, fitted curve: $\langle L \rangle = 0.23 t^{1/3}$ bars show the standard deviation of $P(L_a)$.

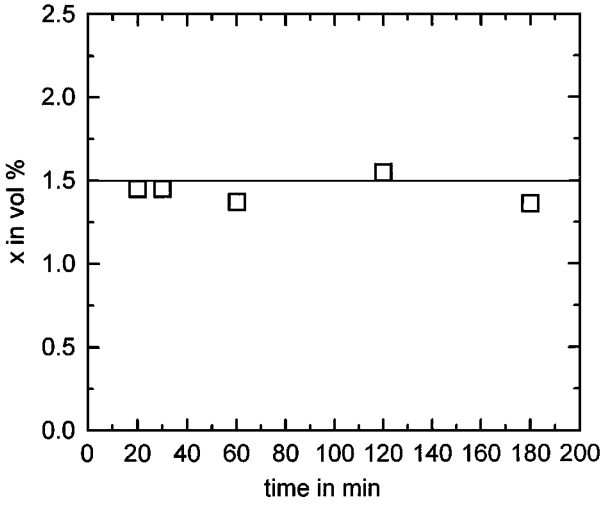

Figure 9 Calculated volume fraction of crystal phase, x, according to Equation 4 for $h = 2\,\mu$m.

4.3. Volume fraction of apatite

One of the typical characteristics of Ostwald ripening is the constancy of the crystal volume fraction. This constancy was indicated by a constant area fraction of apatite crystals in [6], where $25 \pm 5\%$ was reported for all applied thermal treatments. In this work, a similar constant value for the crystalline area fraction of $35 \pm 5\%$ was found. In order to calculate the volume fraction of apatite, x, from electron micrographs, several simplifications were made. Thus, x was approximated for the cylindrical shape of apatite needles as:

$$x = \frac{V_C}{V_0} = \frac{N \cdot A \cdot \frac{\pi}{4}\langle D\rangle^2 \cdot \langle L\rangle}{A \cdot h} \qquad (4)$$

where V_C is the total volume of the crystal phase, V_0 the volume of the "visible" sample layer, h its thickness, A its area, and N the number of crystals per unit square. The results, given in Fig. 9, show a constancy of x. The constancy of x is also indicated by Equation 4 taking into account that $\langle D\rangle \sim t^{-1/3}$, $\langle L\rangle \sim t^{-1/3}$ and $N \sim t^{-1}$ was found. Due to the possible range of $h \approx 2$–$5\,\mu$m [8], however, x remains uncertain between 1.5 and 0.6 vol %. One should note, however, that x can be influenced by washingout of crystals during etching. Thus, larger values of $x \approx 5$–10 vol % were found by X-ray powder diffraction measurements [4]. x can reach even ≈ 19 vol %, as might be anticipated from the chemical composition of the glass and the crystal, assuming $\rho_{glass} \approx 2.5\,\mathrm{g\,cm^{-3}}$ and $\rho_{crystal} \approx 3.2\,\mathrm{g\,cm^{-3}}$ [9].

5. Summary

The coarsening of needle-shaped apatite crystals was studied in a SiO_2 • Al_2O_3 • Na_2O • K_2O • CaO • P_2O_5 • F glass. Lengths, diameters, and numbers of apatite needles were measured by image analysis of electron micrographs. The latter were obtained from fractured powder compacts sintered from differently annealed glass powders. With increasing annealing time, the crystal size increases while the number of crystals decreases and a constant volume fraction of apatite is maintained. Kinetic results indicate that this phenomenon is controlled by Ostwald ripening for diffusion-limited growth mode. Thus, the mean diameter and the mean length of the needles follow a power law of growth according to $\sim t^{1/3}$. A time-invariant reduced size distribution is evident for needle diameters. The measurement of true needle length suffers from several difficulties (e.g. needle orientation). The apparent length distribution could be well fitted for small crystals. Its shape could be attributed to needle orientation phenomena.

Acknowledgement

This work is a part of a co-operative effort of TC 7 of the ICG to advance the understanding of crystallization in multicomponent silicate melts. Advice and discussion by TC7 colleagues I. Szabo and G. Völksch are gratefully acknowledged. The authors thank J. Schmelzer for valuable advice and critical reading of the manuscript. L. A. Hilal gratefully acknowledges financial support from the DAAD.

References

1. I. M. LIFSHITZ and V. V. SLEZOV, *J. Phys. Chem. Solids* **19** (1961) 35.
2. V. RAGHAVAN and M. COHEN, in *Treatise on solid-state chemistry* **5** (1975) 67 (Plenum Press, N.Y.).
3. I. GUTZOW and J. SCHMELZER, *The vitreous state* (Springer, Berlin Heidelberg, 1995).
4. W. HÖLAND, *Phosphorous Res. Bull.* **6** (1996) 111.
5. W. HÖLAND, M. FRANK and V. RHEINBERGER, *J. Non. Cryst. Solids* **180** (1995) 292.
6. B. SCHMIDTHAUSER, Diplomarbeit ETH Zürich (1997).
7. D. FAN and L. CHEN, *J. Am. Ceram. Soc.* **80** (1997) 1773.
8. G. VÖLKSCH, private communication.
9. RÖSSLER, *Lehrbuch der Mineralogie* (Verl. Grundstoffindustrie, Leipzig, 1979).

Received 21 July
and accepted 25 August 1998